Geophysical Journal International

Geophys. J. Int. (2012) **189,** 705–716 doi: 10.1111/j.1365-246X.2012.05391.x

The Italian present-day stress map

Paola Montone, Maria Teresa Mariucci and Simona Pierdominici*

Istituto Nazionale di Geofisica e Vulcanologia, Sezione Sismologia e Tettonofisica, Via di Vigna Murata 605, 00143 *Rome, Italy.*
E-mail: paola.montone@ingv.it

Accepted 2012 January 21. Received 2012 January 19; in original form 2011 June 6

SUMMARY

In this paper, we present a significant update of the Italian present-day stress data compilation not only to improve the knowledge on the tectonic setting of the region or to constrain future geodynamic models, but also to understand the mechanics of processes linked to faulting and earthquakes. In this paper, we have analysed, revised and collected new contemporary stress data from borehole breakouts and we have assembled earthquake and fault data. In total, 206 new quality-ranked entries complete the definition of the horizontal stress orientation and tectonic regime in some areas, and bring new information mainly in Sicily and along the Apenninic belt. Now the global Italian data set consists of 715 data points, including 499 of A–C quality, representing an increase of 37 per cent compared to the previous compilation. The alignment of horizontal stresses measured in some regions, closely matches the ∼N–S first-order stress field orientation of ongoing relative crustal motions between Eurasia and Africa plates. The Apenninic belt shows a diffuse extensional stress regime indicating a ∼NE–SW direction of extension, that we interpret as related to a second-order stress field. The horizontal stress rotations observed in peculiar areas reflect a complex interaction between first-order stress field and local effects revealing the importance of the tectonic structure orientations. In particular, in Sicily the new data delineate a more complete tectonic picture evidencing adjacent areas characterized by distinct stress regime: northern offshore of Sicily and in the Hyblean plateau the alignment of horizontal stresses is consistent with the crustal motions, whereas different directions have been observed along the belt and foredeep.

Key words: Downhole methods; Seismicity and tectonics; Crustal structure; Europe.

INTRODUCTION

The World Stress Map Project compilation and several single papers have clearly demonstrated the existence of first-order stress field (plate-scale) controlled by plate boundary forces, and second-order stress field (regional) controlled by major intraplate stress sources (Müller *et al.* 1992; Zoback 1992; Hillis & Reynolds 2000; Tingay *et al*. 2010b). In areas where high data density is present, a third-order stress field (local) can also be recognized linked to the presence of minor features (i.e. active faults, local inclusions, detachment horizons or density contrasts; Bell 1996; Yale 2003; Tingay *et al*. 2005). Such features may explain stress rotations that can be found not only between two adjacent wells but also in the same well along depth (e.g. Mariucci *et al.* 2002; Carminati *et al.* 2010) as observed when fractures, active faults or mechanically weak zones are crossed by, or close to, a borehole (e.g. Bell *et al.* 1992; Barton & Zoback 1994; Bell 1996; Pierdominici *et al.* 2005, 2011; Tingay *et al*. 2011).

The comprehension of the present-day stress state in tectonically dynamic regions is significant to understand the mechanics of various geological/geophysical processes including faulting and earthquakes (Zoback 1992; Sassi & Faure 1996; Suppe 2007). The determination of *in situ* stress is also one of the most important scientific objectives of deep drilling projects because very often the state of stress in the first 5–10 km of the crust is not revealed by any other data. No deep scientific boreholes have been drilled in Italy to date, but opportunity exists to analyse data from numerous petroleum industry boreholes (e.g. ENI S.p.A.) from throughout the country.

In this paper, we present the most complete and updated contemporary stress map of Italy with particular attention to new data from Sicily, an important region both for past large earthquakes and for oil and gas exploitation. We then depict the pattern of crustal stress emphasizing areas both where we recognize a first- or second-order present-day stress field and where we measure local variations recording the third-order stress field.

DATA PRESENTATION

The data set contains 715 stress indicators (499 best-quality, 101 low-quality and 115 discarded data) including: borehole breakouts

*Now at Helmholtz-Zentrum Potsdam, Deutsches GeoForschungsZentrum GFZ, Potsdam, Germany.

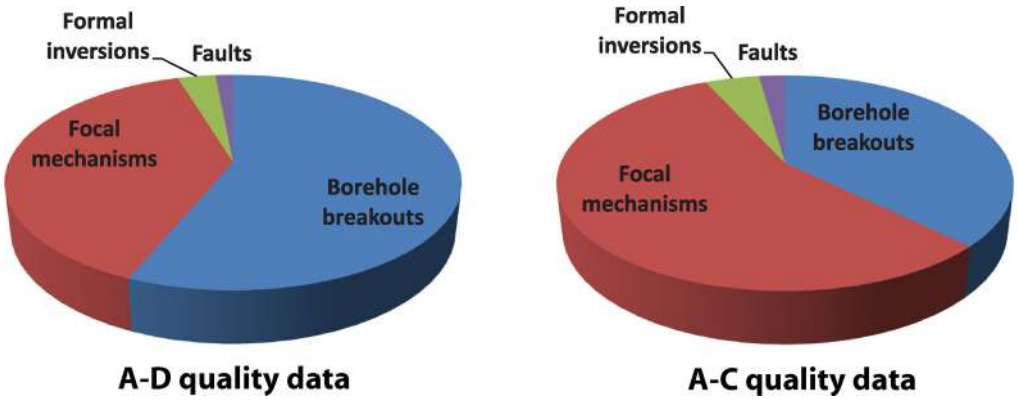

Figure 1. Distribution of stress data by type. The only one overcoring datum is not included.

in deep wells, single earthquake focal mechanisms, formal inversions of focal mechanisms, faults and overcoring data (Fig. 1). A quality ranking between A and E is assigned to each stress data, with A being the highest quality. Following the most up-to-date ranking scheme (Heidbach *et al.* 2010), A-quality indicates that the stress orientation is accurate within $\pm 15^\circ$, B-quality within $\pm 20^\circ$, C-quality within $\pm 25^\circ$ and D-quality within $\pm 40^\circ$. When data do not provide sufficient information or have standard deviations greater than 40°, the data are discarded (E-quality). We use A-, B- and C-quality stress indicators for analysing first-order stress patterns (Heidbach *et al*. 2010) although we also consider D-quality data (actually only breakouts) to define second- or third-order stress field (Montone & Mariucci 1999; Pierdominici *et al*. 2005; Mariucci *et al.* 2008, 2010) as observed in other studies in the world (Tingay *et al.* 2010b).

In the location map (Fig. 2), we report all the new data (see also Tables 1 and 2) to give a general overview of their distribution. Stress information derived from breakouts is widespread along the Italian territory particularly along the Po Plain–Adriatic foredeep, along the southern belt and foredeep and in Sicily; the Apenninic belt is well covered by several moderate magnitude earthquakes and some seismic sequences as well as Sicily and specific areas of northern Italy; finally, fault data usable for stress analysis are located along the central-southern Apennines.

Depth interval of the entire data set is between 0 and 40 km including faults, borehole breakouts and earthquake data. The results are reported in terms of minimum horizontal stress ($S_{\rm hmin}$) both in map (Fig. 3) and in the tables. Concerning breakouts their preferred orientations correspond to $S_{\rm hmin}$; because all the considered faults are normal faults, we assume the $S_{\rm hmin}$ direction as perpendicular to the fault strike, assuming an Andersonian faulting and stress model. Because our seismological data set is mainly characterized by dip-slip faulting mechanisms, the use of principal axis directions (*P*-, *T*- and *N*-axes) can provide a reliable description of the regional stress orientation, consistent with the World Stress Map assumptions (Zoback 1992).

Data from new borehole breakout analysis

Borehole breakouts are stress-induced enlargements of the wellbore cross-section that occur when a well is drilled in rocks in an anisotropic stress field (Bell & Gough 1979; Zoback *et al*. 1985). They develop in two opposite zones of the borehole wall and are aligned along the direction of the minimum horizontal stress. In this work, we determine breakouts by using 'four-arm calliper' tool following the main criteria reported in Plumb & Hickman (1985): that is, the tool rotation ceases along the breakout zone; one of the two callipers is longer than the other one, approximately equal to the bit-size; the hole deviation is less than 15° and the azimuth of breakout is different (by more than 10°) from the hole azimuth. Usually, the breakout zones are plotted as a rose diagram, with bars proportional to cumulative breakout lengths. We apply the circular statistics of Mardia (1972) to compute, for each borehole, the mean breakout orientation and its standard deviation (95 per cent confidence interval) weighed by length of breakout intervals. The WSM quality ranking system (Heidbach *et al.* 2010) used to classify the breakout orientation of each well, from A to E, takes into account the number of breakout zones, the total length of breakouts and the variability of the measurements (standard deviation).

Fig. 2 shows the location of the wells where new breakout analyses have been performed (black and grey dots). We have analysed 20 new wells in Sicily; 3 new wells located in northern Italy and along the Adriatic margin; revised all the 46 data previously used to constrain finite element models (Barba *et al.* 2010); entered 1 well crossing the $M = 6.9$ Irpinia fault (Pierdominici *et al.* 2011); included 2 wells recently analysed after the L'Aquila 2009 earthquake (Mariucci *et al.* 2010) and finally, we added 2 revised wells located in central Apennines (Mariucci *et al.* 2008). In total, we have 74 new entries, 36 of which have reliable A, B and C quality; the minimum depth of breakout data is 450 m and the maximum depth is 5585 m (Table 1).

Data from other sources

In our data set we include also other stress indicators as focal mechanism of earthquakes, formal inversions from diffuse minor seismicity and fault data to define the tectonic regime, explore deeper depth intervals and expand the study areas.

Earthquake focal mechanisms

The previous compilation by Montone *et al.* (2004) collected data up to 2003 June. Now we have considered the period from 2003 July to 2010 December and we have replaced previous Quick Regional CMT (http://autorcmt.bo.ingv.it/quicks.html) with the new computations (Pondrelli *et al.* 2004, 2007, 2010, 2011; RCMT European–Mediterranean Catalog, http://www.bo.ingv.it/RCMT). We take into account CMT-like solutions of earthquakes with $M \geq 4$ and crustal depth within the first 40 km (Table 2). The systematic error that can be associated to principal axis directions (*P*, *T* and

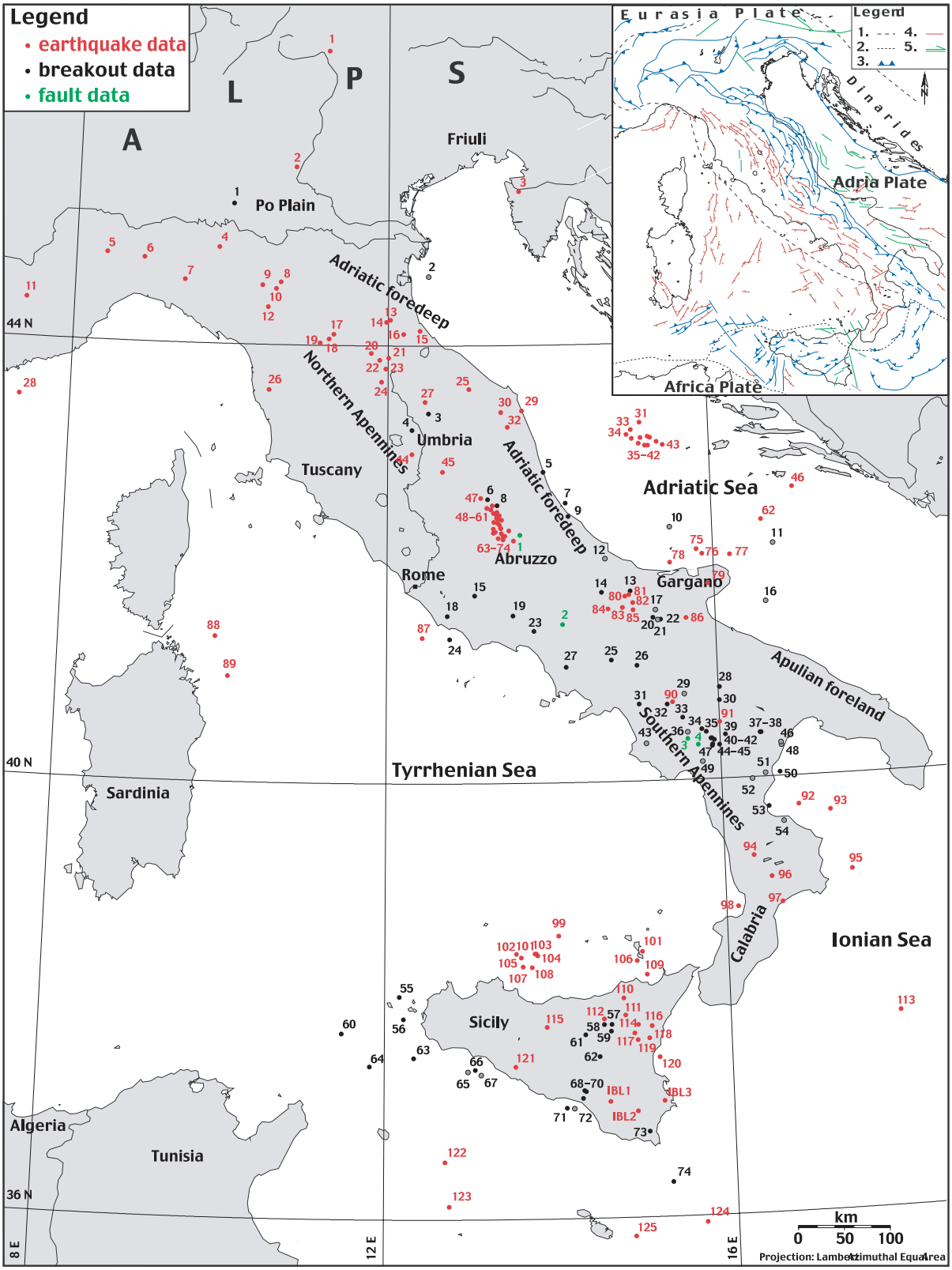

Figure 2. Location map of data presented in this paper. New analysed and revised wells for breakout analysis: black dots are for breakout ranked from A to D quality; grey dots are for data with E quality. Earthquakes are reported as red dots. Faults are green dots. Numbers correspond to data set of Table 1 (breakouts), Table 2 (earthquakes) and Table 3 (faults). Acronyms (IBL1, IBL2 and IBL3) are relative to focal mechanism formal inversions. See text for further explanation and References. Inset: Schematic tectonic map of Italy: (1) border of the continental part of the Adria microplate; (2) border of Adria, Ionian, Sicily and Africa plates; (3) main compressive faults; (4) main extensional faults and (5) main strike-slip faults. Tectonics modified from Meletti *et al.* (2000).

Table 1. Borehole breakout data.

No.	Lat.	Lon.	S_{hmin}	*SD*	Top	Bottom	Q	References
1	45,28	9,97	96	11	1269	1918	A	1
2	44,64	12,48					E	1
3	43,38	12,42	12	29	500	5541	D	2[a]
4	43,23	12,28	55	22	1550	4022	C	2[b]
5	42,84	13,91	33	10	2465	2575	C	1
6	42,60	13,22	81	22	1416	4605	C	3
7	42,56	14,18	25	21	450	2539	C	4
8	42,54	13,34	74	10	1747	2450	C	3[c]
9	42,44	14,22	114	12	493	2816	B	4
10	42,33	15,47					E	4
11	42,15	16,72					E	4
12	42,05	14,66					E	4
13	41,75	14,96	5	10	2217	2670	B	4
14	41,75	14,61	7	27	3927	4081	D	4
15	41,71	13,07	175	18	1268	2520	B	4
16	41,63	16,61					E	4
17	41,57	15,26					E	4
18	41,53	13,53	149	20	600	1977	B	4
19	41,53	12,73	62	11	845	1324	C	4
20	41,50	15,23	6	9	2537	3004	D	4
21	41,48	15,29					E	4
22	41,48	15,32	68	35	955	2262	D	4
23	41,39	13,78	177	24	1946	2035	D	4
24	41,32	12,76	112	34	1250	2396	D	4
25	41,12	14,71	170	22	1518	3408	C	4
26	41,07	15,02	157	8	2440	3038	C	4
27	41,06	14,17	42	35	527	1268	D	4
28	40,86	16,01	69	12	500	1678	C	4
29	40,79	15,58					E	4
30	40,73	16,00	41	14	1250	3198	C	4
31	40,71	15,04	160	26	4120	4268	D	4
32	40,70	15,37	18	24	2000	5585	C	5
33	40,58	15,56	28	29	3155	3968	D	4
34	40,47	15,78	47	26	2037	4290	D	4
35	40,44	15,83	39	17	2355	3200	C	4
36	40,44	15,61					E	4
37	40,42	16,48	72	22	730	1178	C	4
38	40,42	16,49	142	33	977	1446	D	4
39	40,41	16,06	174	17	4340	5500	B	4
40	40,38	15,89	41	11	3226	3947	B	4
41	40,38	15,88	43	24	571	962	C	4
42	40,37	15,92	93	24	3617	4246	C	4
43	40,35	15,12	102	27			E	4
44	40,33	15,90	72	18	2560	3304	B	4
45	40,32	15,99	36	27	1383	2783	D	4
46	40,32	16,72	98	30			E	4
47	40,32	15,90	44	19	835	1069	B	4
48	40,30	16,73					E	4
49	40,17	15,78					E	4
50	40,06	16,71	81	21	3531	3823	C	4
51	40,05	16,52					E	4
52	40,00	16,36					E	4
53	39,74	16,55	92	18	3507	3938	B	4
54	39,60	16,72	177	29			E	4
55	38,03	12,18	30	14	1999	3350	B	1
56	37,83	12,24	104	15	1670	2424	B	1
57	37,78	14,64	11	33	1839	3646	D	1
58	37,78	14,55	99	28	1485	3645	D	1
59	37,72	14,63	154	29	1790	2791	D	1
60	37,69	11,53	38	22	1475	2695	C	1
61	37,68	14,34	132	8	2245	2842	C	1
62	37,48	14,49	134	16	3200	3978	B	1
63	37,47	12,36	102	18	1414	2537	B	1
64	37,39	11,85	33	22	1547	2493	C	1
65	37,37	13,10					E	1
66	37,37	13,07	53	30	2225	2740	D	1
67	37,32	13,13					E	1
68	37,17	14,31	58	0	3412	3525	C	1
69	37,16	14,33	127	22	500	3392	C	1
70	37,10	14,30	92	9	3564	3619	D	1
71	37,01	14,12	114	10	2575	5129	A	1
72	37,01	14,20					E	1
73	36,79	15,05	62	11	932	2615	D	1
74	36,32	15,30	38	9	2009	2564	D	1

S_{hmin}, minimum horizontal stress; *SD*, standard deviation; top, bottom (m) of breakout data; Q, quality (see text).
References: 1, This work; 2, Mariucci *et al.* (2008); 3, Mariucci *et al.* (2010); 4, Barba *et al.* (2010); 5, Pierdominici *et al.* (2011).
[a]Ex no. 99 in Montone *et al.* (2004).
[b]Ex no. 108 in Montone *et al.* (2004).
[c]Ex no. 181 in Montone *et al.* (2004).

N) from CMT-like solutions is ±14° (Helffrich 1997). Moreover, although focal plane solution principal axes could not be indicative of stress axes, the possible differences between S_{hmin} derived from *P*-, *T*- and *N*-axes and S_{hmin} from slip vectors lie within the error of the attributed quality as shown in Montone *et al.* 2004.

Taking into account the systematic error of CMT-like solutions and the range of stress orientations that would be consistent with each focal mechanism and that the orientation of the *P*-, *N*- and *T*-axes could deviate from the principal stress orientations (McKenzie 1969), the World Stress Map project (Heidbach *et al*. 2010) assigns C-quality to focal mechanism data (stress orientations within ±25°). Furthermore, in this paper, the use of principal axis directions (*P*-, *T*- and *N*-axes) is reasonable because we apply this data set to provide regional stress orientations and also we can be confident of other stress indicators.

Concerning the quality value, after the previous compilation (Montone *et al.* 2004), the criteria suggested by the World Stress Map Project have changed. In the last release (www.world-stress-map.org), the quality ranking scheme is more stringent and, especially, all single focal mechanisms have to be considered C quality (stress orientation range ±25°) even if with high magnitude, then all the earthquakes with B quality of the previous compilation have now C quality.

New data are broadly spread along the Italian peninsula (125 new entries), with two areas remarkably improved: Sicily on- and offshore and the Abruzzo region.

The 2009 L'Aquila seismic sequence has improved our data set with: (i) 25 moderate-sized earthquakes showing normal faulting mechanisms with *T*-axis NE-oriented (Table 2; no. 47–61 and 63–74; Pondrelli *et al*. 2010); (ii) NW-oriented surface breaks, not reported in the map and (iii) two deep wells providing a ∼ENE S_{hmin} orientation (Table 1; no. 7, 9; Mariucci *et al*. 2010).

Formal inversions

Stress orientation determined from inversions of *P*-, *T*- and *N*-axes of diffuse seismicity has also been updated with the inclusion of three recent data located in Sicily, in the Hyblean Plateau (Musumeci *et al.* 2005). The formal inversions refer to seismic events from 1994 to 2002 with magnitude M_L 1.0–4.6 and depth interval between 5 and 26 km; IBL1, IBL2 and IBL3 inversions include 22, 23 and

Table 2. Earthquake focal mechanism data.

No.	Lat	Lon	S_{hmin}	Q	TR	D (km)	M	Date	Strike1	Dip1	Rake1	Strike2	Dip2	Rake2	References
1	46,70	11,16	75	C	SS	22,1	4.8	2001 July 17	210	72	7	117	83	162	1
2	45,63	10,76	54	C	TF	15,4	5.0	2004 November 24	235	25	92	53	65	89	2
3	45,42	13,64	120	C	SS	32,9	4.0	2002 June 02	346	76	−179	255	89	−14	1
4	44,88	9,79	63	C	TF	20,0	4.1	2009 October 19	41	43	59	260	54	115	4
5	44,79	8,36	42	C	SS	15,0	4.1	2001 July 18	95	49	179	185	89	41	1
6	44,76	8,84	70	C	SS	15,0	4.8	2003 April 11	297	75	−165	203	75	−16	2
7	44,57	9,37	16	C	NF	13,1	4.0	2005 April 18	336	34	−35	96	71	−118	3
8	44,57	10,60	103	C	TF	35,1	4.2	2002 June 08	301	45	116	86	51	66	1
9	44,54	10,36	110	C	TF	28,0	5.5	2008 December 23	295	34	97	107	56	86	3
10	44,51	10,54	110	C	TF	28,3	4.9	2008 December 23	286	34	84	113	57	94	3
11	44,34	7,36	76	C	NS	10,0	4.1	2008 October 24	308	51	−150	198	67	−43	3
12	44,34	10,44	104	C	TF	35,0	4.3	2002 June 18	293	44	103	95	48	78	1
13	44,24	12,00	95	C	TF	28,0	4.8	2009 April 05	244	41	44	118	63	122	4
14	44,22	11,95	117	C	TF	16,6	4.2	2003 December 07	284	45	71	130	48	108	2
15	44,14	12,37	58	C	SS	35,2	4.1	2010 October 13	17	65	22	278	70	153	4
16	44,11	12,17	178	C	TF	15,0	4.0	2010 September 05	200	43	125	336	56	62	4
17	44,10	11,28	81	C	TF	22,7	5.3	2003 September 14	246	40	68	94	53	107	2
18	44,06	11,22	39	C	NF	10,0	4.2	2008 March 01	326	43	−67	116	51	−110	3
19	44,02	11,11	35	C	NF	10,0	4.7	2008 March 01	278	36	−123	136	60	−168	3
20	43,93	11,76	55	C	NF	10,0	4.5	2003 January 26	291	37	−130	158	62	−64	2
21	43,89	11,98	58	C	NF	10,0	4.7	2003 January 26	140	41	−101	336	50	−80	2
22	43,87	11,86	40	C	NF	10,0	4.1	2002 February 21	313	35	−86	128	55	−93	1
23	43,79	11,94	115	C	TF	35,0	4.5	2006 April 16	295	34	91	114	56	89	3
24	43,67	11,89	71	C	NF	10,0	4.7	2001 November 26	358	21	−72	158	70	−97	1
25	43,61	12,99	79	C	SS	24,4	4.2	2006 October 21	34	60	12	298	80	150	3
26	43,58	10,48	27	C	NF	13,1	4.2	2006 April 17	323	50	−53	94	52	−125	3
27	43,49	12,44	22	C	NF	2,0	4.1	2010 April 15	144	21	−57	288	72	−102	4
28	43,45	7,35	70	C	TF	17,9	4.5	2001 February 25	229	37	60	85	59	111	1
29	43,41	13,65	43	C	SS	21,3	4.1	2006 April 10	89	71	−169	355	80	−20	3
30	43,40	13,39	66	C	SS	37,0	4.7	2009 September 20	21	78	−3	112	87	−168	4
31	43,29	15,12	85	C	TF	15,0	4.3	2003 April 03	105	25	116	256	67	78	2
32	43,26	13,47	6	C	NS	31,0	4.1	2010 January 12	52	48	−161	309	76	−44	4
33	43,22	15,01	101	C	TF	15,0	4.4	2003 April 26	118	48	114	264	48	66	2
34	43,18	14,95	107	C	TF	15,0	4.9	2003 March 27	133	44	128	266	57	59	2
35	43,16	15,22	91	C	TF	10,0	4.2	2003 March 30	99	41	101	264	50	80	2
36	43,15	15,13	89	C	TF	16,0	4.4	2003 June 21	249	40	62	103	56	111	2
37	43,15	15,24	105	C	TF	15,0	4.5	2003 March 31	290	43	97	101	48	84	2
38	43,14	15,02	105	C	TF	15,0	5.3	2004 November 25	111	41	99	280	49	82	2
39	43,11	15,33	138	C	TF	15,0	4.1	2003 May 05	105	52	40	348	60	134	2
40	43,10	15,11	110	C	TF	15,0	5.5	2003 March 29	287	41	85	114	49	95	2
41	43,08	15,19	98	C	TF	15,0	4.6	2004 December 03	279	32	91	97	58	89	2
42	43,08	15,22	103	C	TF	15,0	4.6	2003 March 30	98	43	83	287	47	96	2
43	43,08	15,40	130	C	TF	15,0	4.4	2003 April 29	109	32	61	322	63	107	2
44	43,01	12,28	28	C	SS	15,0	4.2	2009 December 15	163	75	2	72	88	165	4
45	42,85	12,66	86	C	NF	15,0	4.1	2010 August 28	159	44	−113	9	50	−70	4
46	42,66	16,99	118	C	TF	36,9	4.3	2002 October 23	103	43	69	311	50	108	1
47	42,61	13,14	41	C	NF	10,0	4.0	2009 April 14	309	42	−92	132	48	−88	5
48	42,54	13,28	48	C	NF	10,0	4.1	2009 April 15	113	33	−126	333	64	−69	5
49	42,52	13,21	60	C	NF	15,0	4.3	2010 August 31	139	45	−105	340	47	−75	4
50	42,51	13,26	47	C	NF	15,6	5.2	2009 April 09	132	46	−97	321	44	−83	5
51	42,48	13,34	53	C	NF	15,4	5.4	2009 April 09	329	45	−81	136	46	−99	5
52	42,47	13,29	53	C	NF	11,8	5.0	2009 April 13	337	38	−71	133	54	−104	5
53	42,45	13,33	82	C	NF	10,0	4.2	2009 September 24	184	35	−76	347	56	−100	4
54	42,45	13,36	70	C	NF	10,0	4.2	2009 April 05	147	37	−108	349	55	−77	5
55	42,45	13,36	29	C	NF	13,1	4.7	2009 June 22	113	19	−112	315	72	−83	5
56	42,42	13,33	39	C	NF	14,1	4.1	2009 April 08	319	40	−76	121	51	−101	5
57	42,41	13,35	58	C	NS	12,8	4.3	2009 April 09	2	61	−39	113	57	−144	5
58	42,41	13,39	67	C	NF	10,0	4.1	2009 July 03	144	42	−108	348	50	−74	5
59	42,39	13,30	51	C	NF	10,0	4.2	2009 April 06	138	41	−93	323	49	−87	5
60	42,38	13,34	80	C	NF	10,0	4.5	2009 April 06	340	25	−103	175	66	−84	5
61	42,37	13,36	56	C	NF	11,8	5.1	2009 April 06	341	44	−68	132	50	−109	5
62	42,37	16,59	80	C	TF	15,0	4.3	2010 June 04	61	48	62	279	49	117	4
63	42,34	13,38	63	C	NF	10,0	4.3	2009 July 12	342	35	−76	146	56	−99	5
64	42,33	13,29	33	C	NF	11,7	4.5	2009 April 07	321	41	−64	108	54	−110	5

Table 2. (*Continued.*)

No.	Lat	Lon	S_{hmin}	Q	TR	*D* (km)	*M*	Date	Strike1	Dip1	Rake1	Strike2	Dip2	Rake2	References
65	42,33	13,38	78	C	NF	14,0	4.4	2009 March 30	2	35	−70	158	57	−104	5
66	42,31	13,48	44	C	NF	20,5	5.5	2009 April 07	105	53	−134	342	55	−48	5
67	42,30	13,31	49	C	NF	11,6	6.3	2009 April 06	326	35	−80	*134*	*56*	*−97*	5
68	42,29	13,29	59	C	NF	10,8	4.4	2009 April 06	348	40	−64	135	55	−111	5
69	42,29	13,39	60	C	NF	12,9	5.1	2009 April 06	355	46	−53	128	55	−122	5
70	42,26	13,41	53	C	NF	13,6	5.1	2009 April 07	341	41	−64	128	54	−111	5
71	42,26	13,43	25	C	SS	26,0	4.4	2009 April 09	67	50	−170	331	83	−40	5
72	42,24	13,35	57	C	NF	10,0	4.3	2009 April 23	323	27	−95	149	63	−87	5
73	42,23	13,41	70	C	NF	12,2	4.0	2009 April 08	344	38	−84	156	52	−95	5
74	42,22	13,54	46	C	NF	11,0	4.1	2009 April 23	326	49	−76	126	43	−105	5
75	42,12	15,78	49	C	SS	37,8	4.3	2006 October 04	274	79	178	4	89	11	3
76	42,07	15,85	33	C	TS	30,3	4.2	2008 March 19	69	57	145	179	61	38	3
77	42,06	16,19	33	C	TF	33,3	4.5	2006 December 10	28	31	83	217	59	94	3
78	42,00	15,45	51	C	NF	10,0	4.5	2001 July 02	246	19	−166	143	85	−72	1
79	41,80	15,91	65	C	TF	31,8	4.6	2006 May 29	260	39	112	53	55	73	3
80	41,71	14,89	28	C	SS	20,9	4.6	2002 November 12	72	80	171	163	82	10	1
81	41,71	14,94	36	C	SS	16,9	5.7	2002 November 01	170	75	−4	*261*	*86*	*−165*	1
82	41,64	14,99	39	C	SS	17,4	5.7	2002 October 31	174	67	−8	*267*	*82*	*−157*	1
83	41,60	14,86	33	C	SS	18,8	4.5	2003 June 01	167	72	−12	261	79	−162	2
84	41,59	14,68	38	C	SS	26,0	4.5	2002 November 01	263	56	−166	165	78	−35	1
85	41,58	14,99	48	C	SS	15,6	4.5	2003 December 30	187	53	−6	281	85	−142	2
86	41,49	15,63	16	C	NS	30,1	4.3	2010 September 17	148	45	−25	256	73	−132	4
87	41,33	12,43	113	C	SS	16,3	4.8	2005 August 22	341	62	180	71	90	28	3
88	41,31	9,91	164	C	TF	19,1	4.5	2001 November 07	334	29	77	169	62	97	1
89	40,95	10,08	170	C	TF	15,0	4.6	2004 December 18	144	49	51	15	54	126	2
90	40,72	15,44	43	C	NF	15,0	4.4	2002 April 18	340	49	−52	109	54	−126	1
91	40,53	16,00	33	C	TS	35,1	4.1	2006 September 07	178	55	35	66	62	139	3
92	39,75	16,90	166	C	TF	37,0	4.7	2006 June 22	173	44	100	339	47	80	3
93	39,69	17,28	178	C	SS	32,0	4.7	2006 April 17	223	83	177	314	87	7	3
94	39,30	16,35	61	C	NF	10,0	4.3	2001 October 18	332	44	−88	149	46	−92	1
95	39,14	17,49	31	C	SS	38,7	4.5	2008 November 20	166	82	−2	256	88	−172	3
96	39,10	16,55	110	C	NS	16,4	4.4	2008 April 08	235	49	−35	350	64	−134	3
97	38,87	16,66	61	C	SS	15,0	4.4	2010 October 15	287	62	173	20	84	28	4
98	38,83	16,14	164	C	NS	15,0	4.1	2010 June 16	109	50	−38	225	62	−133	4
99	38,59	14,04	72	C	TF	10,0	4.8	2009 September 07	276	41	124	54	57	64	4
100	38,44	13,78	55	C	TF	15,0	5.9	2002 September06	37	42	64	251	53	112	1
101	38,44	15,01	77	C	TF	15,0	4.4	2002 April 05	90	41	108	246	52	75	1
102	38,43	13,54	45	C	TF	15,0	4.4	2002 September10	71	29	126	211	67	72	1
103	38,43	13,77	55	C	TF	15,0	4.9	2002 October 02	33	41	59	252	56	115	1
104	38,42	13,79	47	C	TF	15,0	4.7	2002 September06	252	48	126	24	53	56	1
105	38,40	13,60	70	C	TF	15,0	4.6	2002 September28	79	39	103	243	52	80	1
106	38,36	14,95	87	C	SS	10,0	4.7	2010 August 16	221	73	−6	312	85	−163	4
107	38,31	13,62	55	C	TF	16,1	4.7	2002 September20	46	33	77	241	58	99	1
108	38,31	13,73	55	C	TF	15,0	5.1	2002 September27	41	39	70	246	53	105	1
109	38,23	15,06	117	C	NF	12,0	4.4	2006 February 27	22	24	−95	208	66	−88	3
110	38,02	14,78	59	C	NF	15,0	4.2	2006 December 19	18	16	−40	147	80	−102	3
111	37,87	14,81	110	C	SS	10,0	4.5	2002 October 27	67	54	19	326	75	142	1
112	37,83	14,55	6	C	NF	15,0	4.5	2009 November 08	310	21	−54	92	73	−102	4
113	37,82	17,97	121	C	TF	12,0	4.7	2008 February 21	333	27	134	106	71	71	3
114	37,78	14,94	82	C	SS	15,0	4.3	2009 December 19	119	47	−178	28	89	−43	4
115	37,76	13,90	18	C	NF	10,0	4.7	2001 November 25	137	31	−57	280	64	−108	1
116	37,76	15,11	141	C	SS	2,0	4.2	2010 April 02	274	55	10	178	82	145	4
117	37,70	14,90	94	C	SS	10,0	4.9	2002 October 27	320	60	171	55	82	30	1
118	37,65	15,07	93	C	SS	10,0	4.7	2002 October 29	316	61	−173	223	84	−29	1
119	37,63	14,94	175	C	TS	10,0	4.2	2001 April 22	316	56	27	210	68	143	1
120	37,47	15,18	78	C	NS	10,0	4.2	2002 October 29	207	54	−28	314	68	−141	1
121	37,40	13,53	22	C	SS	37,3	4.2	2008 November 28	337	74	9	245	81	164	3
122	36,52	12,72	38	C	SS	28,0	4.4	2009 March 19	255	48	−180	165	90	−42	4
123	36,11	12,77	44	C	SS	10,0	4.8	2006 November 23	357	70	−2	88	88	−160	3
124	35,95	15,67	53	C	SS	33,3	4.4	2006 November 24	188	82	0	98	90	172	3
125	35,83	14,87	37	C	SS	15,0	4.3	2003 July 07	350	62	4	258	87	152	2

S_{hmin}, minimum horizontal stress; Q, quality (see text); TR, tectonic regime; NF, normal faulting; SS, strike-slip faulting; TF, thrust faulting; TS, thrust/strike-slip faulting; NS, normal/strike-slip faulting; *D*, depth, *M*, magnitude; strike, dip, rake of the two nodal planes, the assumed fault plane in italics. References: 1, Pondrelli *et al.* (2004); 2, Pondrelli *et al.* (2007); 3, Pondrelli *et al.* (2011); 4, European Mediterranean RCMT Catalog (http://www.bo.ingv.it/RCMT/); 5, Pondrelli *et al.* (2010).

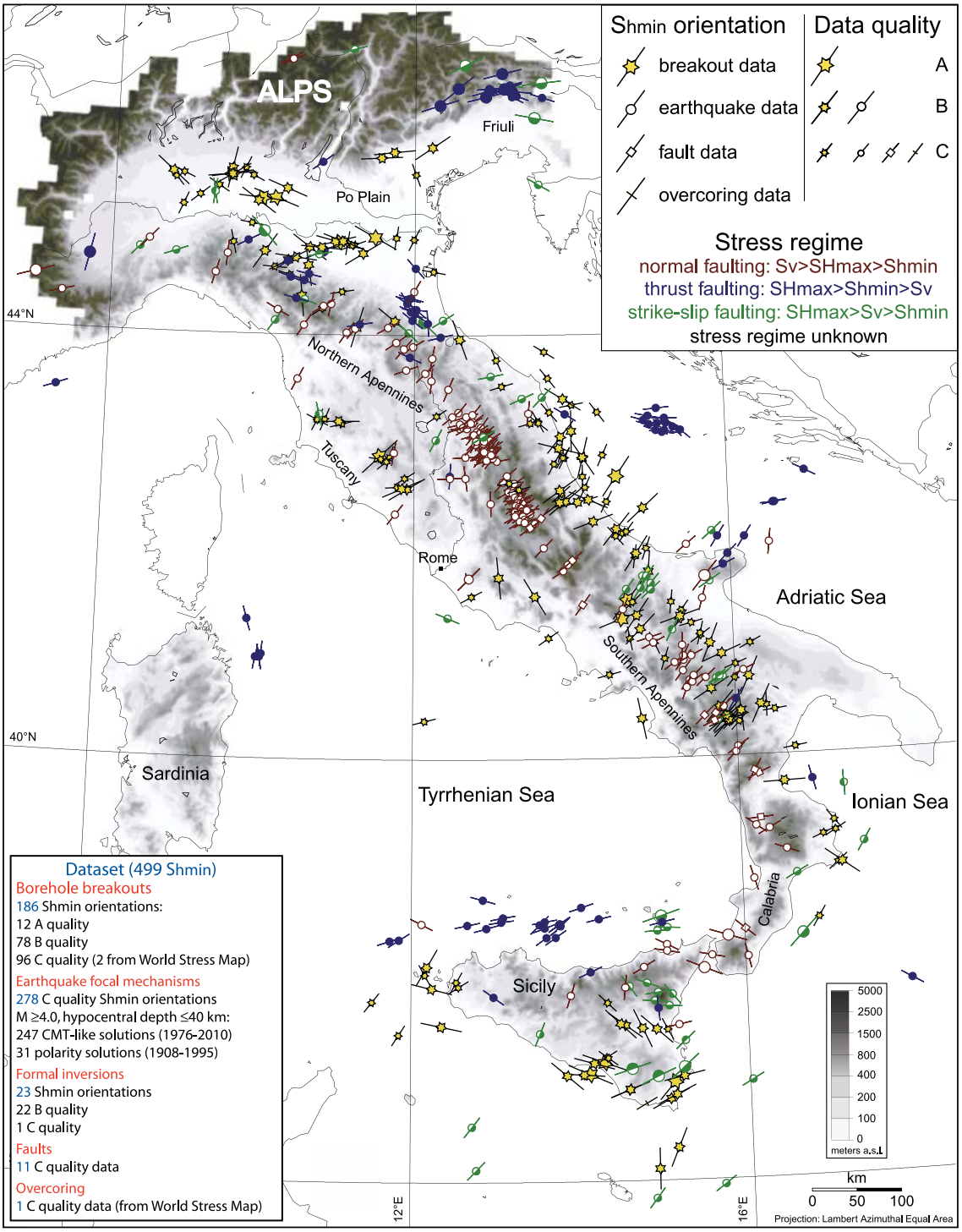

Figure 3. Present day stress map of Italy with minimum horizontal stress orientations (S_{hmin}). Data derive from this paper and from Montone *et al.* (1999, 2004) compilation. Only A–C-quality data are included. Stress map is produced with CASMI (Heidbach & Höhne 2008) which is based on GMT from Wessel & Smith (1998).

25 events, with an average misfit of 4.5°, 6.0° and 5.7°, respectively (Fig. 2).

Fault data

As already described in Montone *et al.* (2004), we do not include faults for which focal mechanisms are available. For this reason we do not enter the 2009 L'Aquila earthquake surface breaks. Whereas, we have considered four new data (Table 3) relative to Melandro–Pergola fault (Moro *et al.* 2007), Aquae Iuliae fault (Galli & Naso 2009), southern Vallo di Diano fault (Villani & Pierdominici 2010) and San Pio fault (Di Bucci *et al.* 2011), although the activity of this latter is still under debate.

Table 3. Fault data.

No.	Lat	Lon	S_{hmin}	Q	TR	Reference
1	42,27	13,62	37	C	NF	Di Bucci *et al.* (2011)
2	41,45	14,13	35	C	NF	Galli & Naso (2009)
3	40,38	15,61	45	C	NF	Moro *et al.* (2007)
4	40,33	15,73	65	C	NF	Villani & Pierdominici (2010)

S_{hmin}, minimum horizontal stress; Q, quality (see text); TR, tectonic regime; NF, normal faulting.

DISCUSSION

The geodynamic setting of the Italian region is characterized by a complex interaction of different processes (Fig. 2), mainly related to the continental collision between Africa and Eurasia plates and the subduction of Adria microplate beneath the Alps (to the north), Dinarides (to the east) and Apennines (to the west). Although Adria is recognized as one of the main features in the central Mediterranean region, its geometry and kinematics are not well defined yet. In fact, according to Anderson & Jackson (1987), Adria would be an independent microplate moving with a counter-clockwise rotation with respect to Eurasia around an Eulerian pole located in northern Italy: this would explain the tectonic extension along the Apenninic belt and the compression in the Eastern Alps and Dinarides. Recently D' Agostino *et al*. (2008), on the basis of a new geodetic model, separate Adria in two main blocks, with two different poles of rotations. The boundary between the blocks would be along the Gargano–Dubrovnik tectonic structure (Westaway 1990; Calais *et al*. 2002; Oldow *et al.* 2002; Battaglia *et al.* 2004), where a diffuse seismicity is recorded. In accordance with this model, the two microplates could explain almost completely the complex tectonic regime along the peninsula. In this context, the Adriatic slab beneath the backarc Tyrrhenian basin, that has caused the migration towards east of extension–compression system along the Apenninic thrust and fold belt (Malinverno & Ryan 1986; Royden *et al*. 1987; Patacca & Scandone 1989; Frepoli & Amato 1997), would assume a less important role with respect to the Neogene evolution of this area, except for the northern Apennines and Calabria arc. In fact, as inferred from deep and intermediate earthquakes and seismic tomography (Selvaggi & Amato 1992; Chiarabba *et al*. 2005; Cimini & Marchetti 2006; Chiarabba *et al*. 2008), the subduction is still active in the southern Tyrrhenian Sea and, possibly, beneath the northern Apennines; whereas, along the central-southern Apennines most of the authors believe that the subduction has ended (e.g. Meletti *et al.* 2000; Di Stefano *et al.* 2009).

In this framework, we distinguish a first-order present-day stress field, associated to Eurasia–Africa Plate motion, in northern Italy (Friuli, Po Plain and Adriatic margin) and in Sicily; a second-order (characterized by a minor wave length) stress field along the extensional Apenninic belt (from Tuscany to Calabria) related to Adria microplate and third-order effects widely spread along the coastal Tyrrhenian margin or localized close to some tectonic structures (i.e. the Irpinia fault, Pierdominici *et al*. 2011).

Present-day stress data, mainly from seismicity, depict a compressive area from the eastern Alps throughout the Po Plain–Adriatic foredeep with two main stress orientations recording the ∼N–S and the ∼NE–SW oblique compression (Fig. 3). In detail, fault plane solutions in Friuli region and subordinately along the Po Plain foredeep are consistent with the Eurasia–Africa convergence, namely the northward push of Adria microplate beneath Europe. Along the Po Plain and the southern Alps front, breakout results confirm S_{hmin} ∼E–W oriented, approximately parallel to the Alpine topographic front, with several localized stress rotations also with depth, related to a sequence of active minor structural arcs (Montone & Mariucci 1999; Selvaggi *et al.* 2001; Burrato *et al.* 2003; Pierdominici *et al.* 2005; Carminati *et al.* 2010). According to Reinecker *et al.* (2010), the same pattern, following the belt trend, is observed in the Molasse Basin (Switzerland and German Alps), confirming the first-order stress field and the role of the deep structure of the Alpine belt in stress rotations.

Along the Adriatic foredeep, close to the northern Apennine thrust front, data indicate NE–SW compression (S_{hmin} ∼NW–SE oriented) consistent, as mentioned earlier, with a still active subducting or sinking slab at depth (Selvaggi & Amato 1992).

On the contrary, in the central part of the foredeep, the remarkable stress change (around latitude 43°N) is linked to a different tectonic regime: S_{hmin} orientations quickly rotate from NW to NE (Fig. 3) evidencing a no longer active compression through the southern foredeep (around latitude 40°N). In this area the absence of intermediate/deep seismicity and clear seismic tomography images suppose that the Adriatic slab is interrupted (Amato *et al*. 1993; Lucente *et al*. 1999; Cimini & Marchetti 2006).

In the inner part of central Italy (Umbria region), the Apenninic belt is characterized by a diffuse extension NE oriented. In particular, the contemporary extension–compression pair evidenced also by our data is probably related to the passive slab retreat (e.g. Malinverno & Ryan 1986; Selvaggi & Amato 1992; Frepoli & Amato 1997; Lucente *et al*. 1999; Faccenna *et al*. 2001; Scrocca *et al*. 2003; Cimini & Marchetti 2006; Di Stefano *et al*. 2009).

Tectonic extension (NE oriented) is also well defined by the data set (seismicity, breakouts and faults) recently achieved in the Abruzzo region, after the destructive M_w 6.3, 2009 earthquake.

Towards south, NE–SW S_{hmin} orientations are well represented and stable along the central-southern Apennines belt and foredeep where several earthquake focal mechanisms depict mainly an extensional and subordinately strike-slip regime, respectively. This section of Italy is characterized by the lack of intermediate earthquakes and also by a continuous high-velocity anomaly depicting the subducted slab. Today is not verified yet if the tomographic images are related to a detached slab or a less pronounced velocity/density anomaly (Amato *et al*. 1993; De Gori *et al*. 2001).

Along the Calabria region crustal stress indicators show an extensional regime with a radial pattern of stress orientations always perpendicular to the main tectonic structures. At depth, the evidence of a subducting slab is very clear from both seismological and geological data, with a well-defined geometry characterized by a narrow, long, downdip compression slab of oceanic Ionian lithosphere (amongst many others, Piana Agostinetti & Amato 2009 and reference therein).

In the Gargano area, data from seismicity have largely increased with respect to the previous map, indicating NE-oriented S_{hmin} mainly related to compressional and strike-slip tectonic regime (i.e. E–W right–lateral nodal planes, no. 81 and 82 in Table 2; Fig. 3). These data can strengthen the hypothesis of a tectonic lineament, ∼ENE-oriented from Gargano to the Dinarides, possibly splitting the Adria microplate in two blocks (Westaway 1990; Calais *et al.* 2002; Oldow *et al.* 2002; Battaglia *et al.* 2004; D'Agostino *et al*. 2008). In central Adriatic, new data related to compressive earthquakes highlight another possible disengagement area of the Adria.

New breakout data along the Tyrrhenian margin (from Rome towards 40°N) show two different S_{hmin} orientations (Fig. 3): a prevalent NE and subordinately NNW, revealing a poor constrained current stress field that we believe is linked to similar horizontal stress magnitudes. We associate this stress pattern to the presence of a local stress field characterized by a predominant vertical stress.

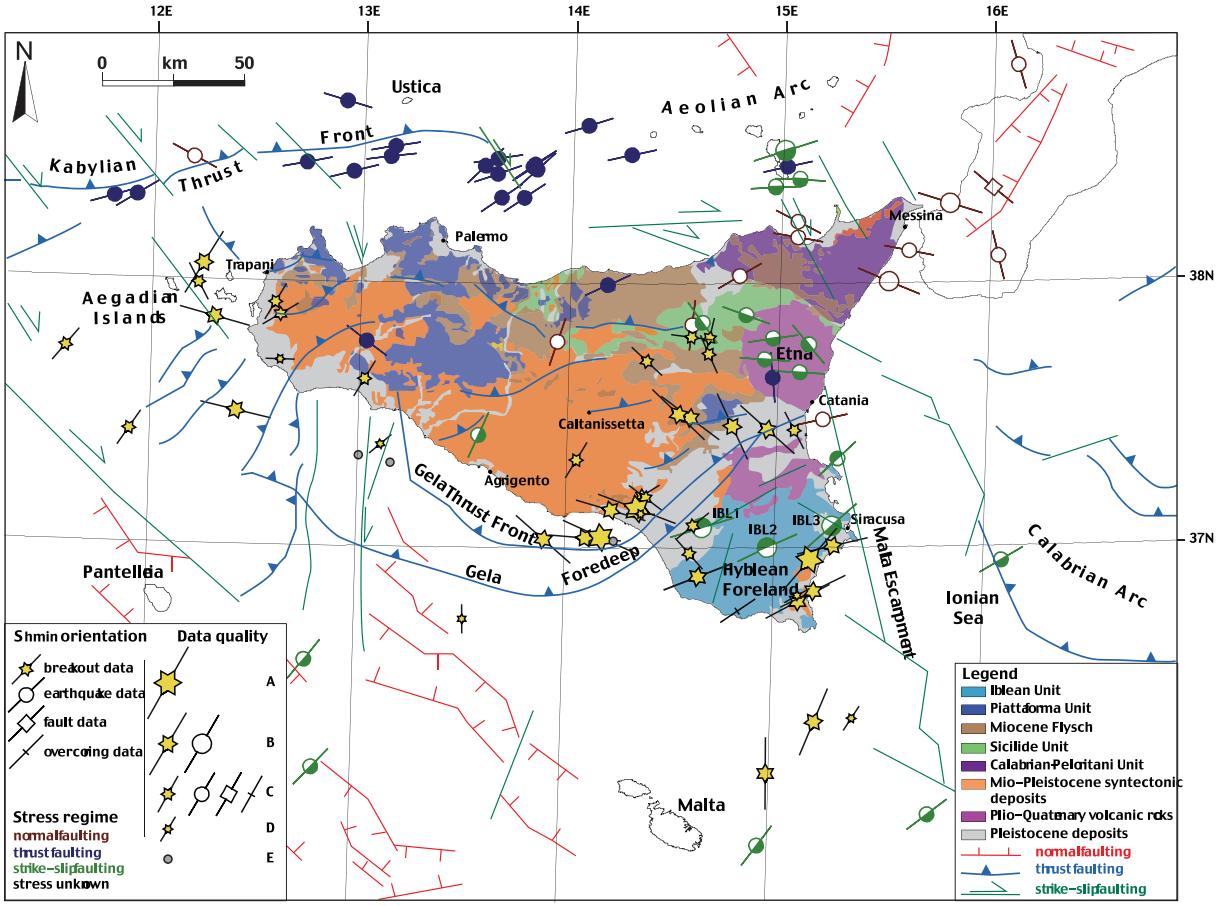

Figure 4. Contemporary stress in the Sicily region: all quality borehole breakout data compared with other stress indicators, tectonics and geology. Geological features simplified from Accaino *et al.* (2011); tectonics simplified and modified from Meletti *et al.* (2000) and Accaino *et al.* (2011).

The most significant increase in the data set is in Sicily both regarding breakouts and earthquakes (Fig. 4). In this case, to discuss the stress pattern of the region we have also plotted D-quality breakout data to highlight local stress field effects. In fact, as several authors have argued (e.g. Tingay *et al.* 2010a,b) D-quality data may best reflect local stress variations and sometimes may provide insight to larger scale stress fields. In particular along the northern offshore of Sicily (Kabylian–Calabrian thrust front), several earthquakes, with prevalent reverse focal mechanisms, describe a clear ∼NNW–SSE current compression (Fig. 4). In southeastern Sicily (Fig. 4), breakout results along the Hyblean foreland are all consistent with ENE-oriented S_{hmin} (Ragg *et al.* 1999; Montone *et al.* 2004). It is worth noting that although presently the Hyblean Plateau shows a low level of instrumental seismicity, in the past strong earthquakes have occurred with a magnitude up to 7.4 (http://emidius.mi.ingv.it/CPTI04). A detailed analysis of earthquakes ($1.0 \leq M_{\mathrm{L}} \leq 4.6$), recorded from 1994 to 2002 in southeastern Sicily (Musumeci *et al.* 2005), has evidenced NNW–SSE compression from predominately strike-slip focal mechanisms. From these data, the authors have computed three formal inversions of earthquakes, whose results are included in this paper (IBL1, 2 and 3 in Fig. 4), indicating a stress regime characterized by S_{hmin} ENE oriented. Then, contemporary stress indicators along the active Kabylian–Calabrian thrust front and within the Hyblean foreland showing a consistent NNW–SSE maximum horizontal stress orientation are in agreement to global plate-motion studies (NUVEL-1, De Mets *et al.* 1990) that predict a ∼340°N convergence between Africa and Eurasia. The localized compression in these two areas points out that the northward Africa push dominates in this part of Sicily.

Along the Gela thrust front (no longer active) breakouts describe its complex structure with several rotations that follow the curved trend of the front itself, almost always pointing perpendicularly to it (Fig. 4). Similar stress rotations have been also observed along active thrust fronts, for instance, offshore NW Borneo collisional margin (King *et al.* 2010) and along the fold and thrust mountain range in New Guinea (Hillis & Reynolds 2000).

Some normal faulting earthquakes showing a WNW–ESE extension suggest that eastern Sicily and southern Calabria (Fig. 4) are dominated by an incipient rifting (Catalano *et al.* 2008). Extension is commonly interpreted as the result of different directions and rates of motion between Sicily and Calabria (Hollenstein *et al.* 2003; D'Agostino & Selvaggi 2004).

We also highlight the occurrence of several strike-slip focal mechanisms (∼E–W-oriented *T*-axis) between the Aeolian Arc and Etna volcano (Fig. 4) that can strengthen the hypothesis of a transfer zone in this area (Billi *et al.* 2010). Towards south, the NNW striking Malta escarpment (Bianca *et al.* 1999; Argnani & Bonazzi 2005 and reference therein) delineates the boundary between the Ionian Sea and the Hyblean foreland (Casero & Roure 1994; Nicolich *et al.* 2000). Results from multichannel seismic data show that active extensional faults (NNW–SSE trending) are present only in the Malta escarpment northern portion (Argnani & Bonazzi 2005). Few data from earthquakes indicate in this area a predominant strike-slip

component with ∼NE-oriented *T*-axis supposing the coexistence of extensional and strike-slip deformation.

CONCLUSIONS

This paper presents the latest significant updating and complete collection of data on the present-day stress orientations in Italy. The achieved map (Fig. 3) can be employed by many users that not only work on this topic and/or related ones such as geophysical modelling, seismic hazard assessment, rock mechanics laboratory experiments, deep drillings, but also on oil and gas well production and construction of nuclear waste deposits.

In some areas of Italy (Sicily, Friuli and Po Plain), the alignment of horizontal stresses closely matches the ∼N–S direction of ongoing crustal motions with respect to stable Europe. This result can be associated to the first-order stress field that drives the plate movement. Along the entire Apenninic belt, from north to south, a diffuse extensional stress regime is clearly showed by a large and broad data set indicating a NE–SW direction of extension, probably related to a second-order stress field.

The stress rotations observed in some areas (i.e. Po Plain minor arcs and Gela thrust front in Sicily) reflect a complex interaction between first-order stress field and local effects that perturb the large-scale regional stress, revealing the importance of the tectonic structure orientations. In particular, in Sicily the new data delineate a more complete tectonic picture highlighting adjacent areas characterized by distinct stress regimes. In this study, the use of stress data of all qualities has been essential for identifying small-scale stress variations. The small-scale changes in the stress orientations, and in some cases also in tectonic regime, over distances of a few tens of kilometres indicate complex t'ectonic processes and interactions amongst different stress field orders.

ACKNOWLEDGMENTS

This work has been carried out in the framework of the following Projects: FIRB Project 'Research and Development of New Technologies for Protection and Defense of Territory from Natural Risks', W.P. C3 'Crustal Imaging in Italy' coordinated by PM, funded by Italian Ministry of University and Research; INGV-DPC Project S1, coordinated by S. Barba and C. Doglioni, funded by Italian Presidenza del Consiglio dei Ministri – Dipartimento della Protezione Civile (DPC). ENI S.p.A. is thanked for providing borehole data. We would like to thank Alessandro Amato for a careful review of the paper and Silvia Pondrelli for the discussion on earthquake focal mechanisms. Many thanks are also due to two anonymous referees for detailed comments that largely improved the manuscript.

REFERENCES

Accaino, F. *et al.*, 2011. A crustal seismic profile across Sicily, *Tectonophysics,* **508**(1–4), 52–61, doi:10.1016/j.tecto.2010.07.011.

Anderson, H. & Jackson, J., 1987. Active tectonics of the Adriatic region, *Geophys. J. R. astr. Soc.,* **91,** 937–987.

Amato, A., Alessandrini, B., Cimini, G.B., Frepoli, A. & Selvaggi, G., 1993. Active and remnant subducted slabs beneath Italy: evidence from seismic tomography and seismicity, *Annali di Geofisica,* **36**2 201–214.

Argnani, A. & Bonazzi, C., 2005. Tectonics of Eastern Sicily Offshore, *Tectonics,* **24,** TC4009, doi:10.1029/2004TC001656.

Barba, S., Carafa, M.M.C., Mariucci, M.T., Montone, P. & Pierdominici S., 2010. Present-day stress-field modelling of southern Italy constrained by stress and GPS data, *Tectonophysics,* **482**(1–4), 193–204, doi:10.1016/j.tecto.2009.10.017.

Barton, C.A. & Zoback, M.D., 1994. Stress perturbations associated with active faults penetrated by boreholes: evidence for near complete stress drop and a new technique for stress magnitude measurement, *J. geophys. Res.,* **99,** 9373–9390, doi:10.1029/93JB03359.

Battaglia, M., Murray, M.H., Serpelloni, E. & Bürgmann, R., 2004. The Adriatic region: an independent microplate within the Africa-Eurasia collision zone. *Geophys. Res. Lett.,* **31,** L09605, doi:10.1029/2004GL019723.

Bell, J.S., 1996. In situ stresses in sedimentary rocks (part 2): applications of stress measurements, *Geosci. Canada,* **23**(3), 135–153.

Bell, J.S. & Gough, D.I., 1979. Northeast-southwest compressive stress in Alberta: evidence from oil wells, *Earth planet. Sci. Lett.,* **45,** 475–482.

Bell, J.S., Caillet, G. & Adams, J., 1992. Attempts to detect open fractures and non-sealing faults with dipmeter logs, *Geol. Soc. Lond. Spec. Publ.,* **65,** pp. 211–220, doi:10.1144/GSL.SP.1992.065.01.16.

Bianca, M., Monaco, C., Tortorici, L. & Cernobori, L., 1999. Quaternary normal faulting in southeastern Sicily (Italy): a seismic source for the 1693 large earthquake, *Geophys. J. Int.,* **139,** 370–394, doi:10.1046/j.1365-246x.1999.00942.x.

Billi, A., Presti, D., Orecchio, B., Faccenna, C. & Neri, G., 2010. Incipient extension along the active convergent margin of Nubia in Sicily, Italy: Cefalù-Etna seismic zone, *Tectonics,* **29,** TC4026, doi:10.1029/2009TC002559.

Burrato, P., Ciucci, F. & Valensise, G., 2003. An inventory of river anomalies in the Po Plain, Northern Italy: evidence for active blind thrust faulting, *Ann. Geophys.,* **46**(5), 865–882.

Calais, E., Noquet, J.M., Jouanne, F. & Tardy, M., 2002. Current strain regime in the Western Alps from continuous Global Positioning System measurements, 1996–2001, *Geology,* **30**(7), 651–654.

Carminati, E., Scrocca, D. & Doglioni, C., 2010. Compaction-induced stress variations with depth in an active anticline: northern Apennines, Italy, *J. geophys. Res.,* **115,** B02401, doi:10.1029/2009JB006395.

Casero, P. & Roure, F., 1994. Neogene deformations at the Sicilian-North African Plate boundary, in *Peri-Tethyan Platforms,* pp. 27–50, ed. Roure, F., Edition Technip, Paris.

Catalano, S., De Guidi, G., Monaco, C., Tortorici, G. & Tortorici, L., 2008. Active faulting and seismicity along the Siculo-Calabrian Rift Zone (Southern Italy), *Tectonophysics,* **453,** 177–192.

Chiarabba, C., Jovane, L. & Di Stefano, R., 2005. A new view of Italian seismicity using 20 years of instrumental recordings, *Tectonophysics,* **395,** 251–268, doi:10.1016/j.tecto.2004.09.013.

Chiarabba, C., De Gori, P. & Speranza, F., 2008. The southern Tyrrhenian subduction zone: deep geometry, magmatism and Plio-Pleistocene evolution, *Earth planet. Sci. Lett.,* **268**(3–4), 408–423, doi:10.1016/j.epsl.2008.01.036.

Cimini, G.B. & Marchetti, A., 2006. Deep structure of peninsular Italy from seismic tomography and subcrustal seismicity, *Ann. Geophys.,* **49**(1), 331–345.

D'Agostino, N. & Selvaggi, G., 2004. Crustal motion along the Eurasia-Nubia plate boundary in the Calabrian Arc and Sicily and active extension in the Messina Straits from GPS measurements, *J. geophys. Res.,* **109,** B11402, doi:10.1029/2004JB002998.

D'Agostino, N., Avallone, A., Cheloni, D., D'Anastasio, E., Mantenuto, S. & Selvaggi, G., 2008. Active tectonics of the Adriatic region from GPS and earthquake slip vectors, *J. geophys. Res.,* **113,** B12413, doi:10.1029/2008JB005860.

De Gori, P., Cimini, G., Chiarabba, C., De Natale, G., Troise, C. & Deschamps, A., 2001. Teleseismic tomography of Campanian Volcanic area and surrounding Apenninic belt, *J. Volc. Geotherm. Res.,* **109**(1–3), 52–75.

De Mets, C., Gordon, R.G., Argus, D.F. & Stein, S., 1990. Current plate motions, *Geophys. J. Int.,* **101,** 425–478.

Di Bucci, D., Vannoli, P., Burrato, P., Fracassi, U. & Valensise, G., 2011. Insights from the Mw 6.3, 2009 L'Aquila earthquake (Central Apennines)—unveiling new seismogenic sources through their surface signatures: the

adjacent San Pio Fault, *TerraNova,* **23**(2), 108–115, doi:10.1111/j.1365-3121.2011.00990.x.

Di Stefano, R., Kissling, E., Chiarabba, C., Amato, A. & Giardini, D., 2009. Shallow subduction beneath Italy: three-dimensional images of the Adriatic-European-Tyrrhenian lithosphere system based on high-quality P wave arrival times, *J. geophys. Res.,* **114,** B05305, doi:10.1029/2008JB005641.

Faccenna, C., Becker, T.W., Lucente, F. P., Jolivet, L. & Rossetti, F., 2001. History of subduction and back-arc extension in the central Mediterranean, *Geophys. J. Int.,* **145,** 809–820.

Frepoli, A. & Amato, A., 1997. Contemporaneous extension and compression in the northern Apennines from earthquake fault-plane solutions, *Geophys. J. Int.,* **129,** 368–388.

Galli, P. & Naso, G., 2009. Unmasking the 1349 earthquake source (southern Italy). Paleoseismological and archaeoseismological indications from the Aquae Iuliae fault, *J. Struct. Geol.,* **31,** 128–149.

Heidbach, O. & Höhne, J., 2008. CASMI—a tool for the visualization of the World Stress Map data base, *Comput. Geosci.,* **34,** 783–791, doi:1016/j.cageo.2007.06.004.

Heidbach, O., Tingay, M., Barth, A., Reinecker, J., Kurfeß, D. & Müller, B., 2010. Global crustal stress pattern based on the World Stress Map database release 2008, *Tectonophysics,* **482,** 3–15, doi:10.1016/j.tecto.2009.1007.1023.

Helffrich, G.R., 1997. How good are routinely determined focal mechanisms? Empirical statistics based on a comparison of Harvard, USGS and ERI moment tensors, *Geophys. J. Int.,* **131,** 741–750.

Hillis, R.R. & Reynolds, S.D., 2000. The Australian stress map, *J. geol. Soc. Lond.,* **157,** 915–921.

Hollenstein, C., Kahle, H.G., Geiger, A., Jenny, S., Goes, S. & Giardini, D., 2003. New GPS constraints on the Africa-Eurasia plate boundary zone in southern Italy, *Geophys. Res. Lett.,* **30,** 1935, doi:10.1029/2003GL017554.

King, R.C., Tingay, M.R.P., Hillis, R.R., Morley, C.K. & Clark, J., 2010. Present-day stress orientations and tectonic provinces of the NW Borneo collisional margin, *J. geophys. Res.,* **115,** B10415, doi:10.1029/2009JB006997.

Lucente, F., Chiarabba, C., Cimini, G. & Giardini, D., 1999. Tomographic constraints on the geodynamic evolution of the Italian region, *Geophys. Res. Lett.,* **104,** 20307–20327.

Malinverno, A. & Ryan, W., 1986. Extension in the Tyrrhenian Sea and shortening in the Apennines as result of arc migration driven by sinking of the lithosphere, *Tectonics,* **5**(2), 227–245, doi:10.1029/TC005i002p00227.

Mardia, K.V., 1972. *Statistics of Directional Data,* Academic Press, San Diego, CA.

Mariucci, M.T., Amato, A., Gambini, R., Giorgioni M. & Montone, P., 2002. Along-depth stress rotations and active faults: an example in a 5-km deep well of Southern Italy, *Tectonics,* **21**(4), 1021, doi:10.1029/2001TC001338.

Mariucci, M.T., Montone, P. & Pierdominici, S., 2008. Active stress field in central Italy: a revision of deep well data in the Umbria region, *Ann. Geophys.,* **51**(2–3), 433–442.

Mariucci, M.T., Montone, P. & Pierdominici, S., 2010. Present-day stress in the surroundings of 2009 L'Aquila seismic sequence (Italy), *Geophys. J. Int.,* **182**(2), 1096–1102, doi:10.1111/j.1365-246X.2010.04679.x.

McKenzie, D.P., 1969. The relation between fault plane solutions for earthquakes and the directions of the principal stress, *Bull. seism. Soc. Am.,* **59,** 591–601.

Meletti, C., Patacca, E. & Scandone, P., 2000. Construction of a seismotectonic model: the case of Italy, *Pageoph,* **157,** 11–35.

Montone, P. & Mariucci, M.T., 1999. Active stress in the NE external margin of the Apennines: the Ferrara arc, northern Italy, *J. Geodyn.,* **28**(2–3), 251–265.

Montone, P., Amato, A. & Pondrelli, S., 1999. Active stress map of Italy, *J. geophys. Res.,* **104,** 25595–25610.

Montone, P., Mariucci, M.T., Pondrelli, S. & Amato, A., 2004. An improved stress map for Italy and surrounding regions (central Mediterranean), *J. geophys. Res.,* **109,** B10410, doi:10.1029/2003JB002703.

Moro, M. *et al.*, 2007. Surface evidence of active tectonics along the Pergola-Melandro fault: a critical issue for the seismogenic potential of the southern Apennines, Italy, *J. Geodyn.,* **44**(1–2), 19–32, doi:10.1016/j.jog.2006.12.003.

Müller, B., Zoback, M.L., Fuchs, K., Mastin, L., Gregersen, S., Pavoni, N., Stephansson, O. & Ljunggren, C., 1992. Regional pattern of tectonic stress in Europe, *J. geophys. Res.,* **97**, 11783–11803.

Musumeci, C., Patanè, D., Scarfì, L. & Gresta, S., 2005. Stress directions and shear-wave anisotropy: observations from local earthquakes in southeastern Sicily, Italy, *Bull. seism. Soc. Am.,* **95**(4), 1359–1374, doi:10.1785/0120040108.

Nicolich, R., Laigle, M., Hirn, A., Cernobori, L. & Gallart, J., 2000. Crustal structure of the Ionian margin of Sicily: Etna volcano in the frame of regional evolution, *Tectonophysics,* **329,** 121–139.

Oldow, J.S. *et al.*, 2002. Active fragmentation of Adria, the north Africa promontory, central Mediterranean orogen, *Geology,* **30**(9), 779–782, doi:10.1130/0091-7613(2002)030<0779:AFOATN>2.0.CO;2.

Patacca, E. & Scandone, P., 1989. Post-Tortonian mountain building in the Apennines. The role of passive sinking of a relic lithospheric slab, in *The Lithosphere in Italy: Advances in Earth Science Research,* pp. 157–176, eds Boriani *et al*., Accademia Nazionale dei Lincei, Rome.

Piana Agostinetti, N. & Amato, A., 2009. Moho depth and Vp/Vs ratio in peninsular Italy from teleseismic receiver functions, *J. geophys. Res.,* **114,** B06303, doi:10.1029/2008JB005899.

Pierdominici, S., Mariucci, M.T., Montone, P. & Cesaro, M., 2005. Comparison between active stress field and tectonic structures in Northern Italy, Lombardy Region, *Ann. Geophys.,* **48**(6), 867–881.

Pierdominici, S., Mariucci, M.T. & Montone, P., 2011. A study to constrain the geometry of an active fault in southern Italy through borehole breakouts and downhole logs, *J. Geodyn.,* **52**(3–4), 279–289, doi:10.1016/j.jog.2011.02.006.

Plumb, R.A. & Hickman, S.H., 1985. Stress-induced borehole elongation: a comparison between the four-arm dipmeter and the borehole televiewer in the Auburn geothermal well, *J. geophys. Res.,* **90**(B7), 5513–5521, doi:10.1029/JB090iB07p05513.

Pondrelli, S., Morelli, A. & Ekström, G., 2004. European-Mediterranean regional centroid-moment tensor catalog: solutions for years 2001 and 2002, *Phys. Earth planet. Inter.,* **145,** 127–147, doi:10.1016/j.pepi.2004.03.008.

Pondrelli, S., Salimbeni, S., Morelli, A., Ekström, G. & Boschi, E., 2007. European-Mediterranean Regional Centroid Moment Tensor catalog: solutions for years 2003 and 2004, *Phys. Earth planet. Inter.,* **164,** 90–112, doi:10.1016/j.pepi.2007.05.004.

Pondrelli, S., Salimbeni, S., Morelli, A., Ekström, G., Olivieri, M. & Boschi, E., 2010. Seismic moment tensors of the April 2009, L'Aquila (Central Italy), earthquake sequence, *Geophys. J. Int.,* **180,** 238–242, doi:10.1111/j.1365-246X.2009.04418.x.

Pondrelli, S., Salimbeni, S., Morelli, A., Ekström, G., Postpischl, L., Vannucci, G. & Boschi, E., 2011. European–Mediterranean Regional Centroid Moment Tensor catalog: solutions for 2005–2008, *Phys. Earth planet. Inter.,* **185,** 74–81, doi:10.1016/j.pepi.2011.01.007.

Ragg, S., Grasso, M. & Müller, B., 1999. Patterns of tectonic stress in Sicily from borehole breakout observation and finite element modeling, *Tectonics,* **18**(4), 669–685.

Reinecker, J., Tingay, M., Müller, B. & Heidbach, O., 2010. Present-day stress orientation in the Molasse Basin, *Tectonophysics,* **482,** 129–138, doi:10.1016/j.tecto.2009.07.021.

Royden, L., Patacca, E. & Scandone, P., 1987. Segmentation and configuration of subducted lithosphere in Italy: an important control on thrust-belt and foredeep-basin evolution, *Geology,* **5,** 714–717.

Sassi, W. & Faure, J.L., 1996. Role of faults and layer interfaces on the spatial variation of stress regimes in basins: inferences from numerical modeling, *Tectonophysics,* **266,** 101–119, doi:10.1016/S0040-1951(96)00185-0.

Scrocca, D., Doglioni, C., Innocenti, F., Manetti, P., Mazzotti, A., Bertelli, L., Burbi, L. & Doffizi, S.,eds, 2003. *CROP Atlas: Seismic Reflection Profiles of the Italian Crust, Volume 1,* Mem. Descr. Carta Geol. It. Vol. 62, Istituto Poligrafico e Zecca dello Stato, Rome., 194p.

Selvaggi, G. & Amato, A., 1992. Subcrustal earthquakes in the northern Apennines (Italy): evidence for a still active subduction? *Geophys. Res. Lett.,* **19,** 2127–2130.

Selvaggi, G. *et al.*, 2001. The M_w 5.4 Reggio Emilia 1996 earthquake: active compressional tectonics in the Po Plain, Italy, *Geophys. J. Int.,* **144,** 1–13.

Suppe, J., 2007. Absolute fault and crustal strength from wedge tapers, *Geology,* **35,** 1127–1130, doi:10.1130/G24053A.1.

Tingay, M.R.P., Hillis, R.R., Morley, C.K., Swarbrick, R.E. & Drake, S.J., 2005. Present-day stress orientation in Brunei: a snapshot of 'prograding tectonics' in a Tertiary delta, *J. geol. Soc. Lond.,* **162**(39), 39–49, doi:10.1144/0016-764904-017.

Tingay, M.R.P., Morley, C., Hillis, R.R. & Meyer, J.J., 2010a. Present-day stress orientation in Thailand's basins, *J. Struct. Geol.,* **32,** 235–248, doi:10.1016/j.jsg.2009.11.008.

Tingay, M., Morley, C., King, R., Hillis, R., Coblentz, D. & Hall, R., 2010b. Present-day stress field of Southeast Asia, *Tectonophysics,* **482,** 92–104, doi:10.1016/j.tecto.2009.06.019.

Tingay, M., Bentham, P., De Feyter, A. & Kellner, A., 2011. Present-day stress-field rotations associated with evaporites in the offshore Nile Delta, *Geol. Soc. Am. Bull.,* **123**(5–6), 1171–1180, doi:10.1130/B30185.1.

Villani, F. & Pierdominici, S., 2010. Late Quaternary tectonics of the Vallo di Diano basin (southern Apennines, Italy), *Quat. Sci. Rev.,* **29**(23–24), 3167–3183, doi:10.1016/j.quascirev.2010.07.003.

Wessel, P. & Smith, W.H.F., 1998. New, improved version of the generic mapping tools released, *EOS, Trans. Am. geophys. Un.,* **79,** 579, doi:10.1029/98EO00426.

Westaway, R., 1990. Present-day kinematics of the plate boundary zone between Africa and Europe, from the Azores to the Aegean, *Earth planet. Sci. Lett.,* **96,** 393–406.

Yale, D.P., 2003. Fault and stress magnitude controls on variations in the orientation of in situ stress, *Geol. Soc. Lond. Spec. Publ.,* **209,** 55–64, doi:10.1144/GSL.SP.2003.209.01.06.

Zoback, M.D., Moos, D., Mastin, L. & Anderson, R.N., 1985. Wellbore breakouts and in situ stress, *J. geophys. Res.,* **90,** 5523–5530.

Zoback, M.L., 1992. First- and second-order patterns of stress in the lithosphere: the world stress map project, *J. geophys. Res.,* **97**(B8), 703–728.